

# JGR Atmospheres

## RESEARCH ARTICLE

10.1029/2023JD038658

### Key Points:

- Circulation Patterns (CPs) provide a new perspective of the lengthening of the dry season in southern Amazonia
- General circulation models (GCMs) show significant future changes in the main dry-to-wet transitional atmospheric states
- GCMs indicate a projected increase in the frequency of CPs typically observed during the Amazon dry season by the mid-21st century

### Supporting Information:

Supporting Information may be found in the online version of this article.

### Correspondence to:

J. Agudelo,  
[jhoana.agudelo-rendon@univ-grenoble-alpes.fr](mailto:jhoana.agudelo-rendon@univ-grenoble-alpes.fr)




### Citation:

Agudelo, J., Espinoza, J. C., Junquas, C., Arias, P. A., Sierra, J. P., & Olmo, M. E. (2023). Future projections of low-level atmospheric circulation patterns over South Tropical South America: Impacts on precipitation and Amazon dry season length. *Journal of Geophysical Research: Atmospheres*, 128, e2023JD038658. <https://doi.org/10.1029/2023JD038658>

Received 7 FEB 2023

Accepted 26 OCT 2023

## Future Projections of Low-Level Atmospheric Circulation Patterns Over South Tropical South America: Impacts on Precipitation and Amazon Dry Season Length

Jhoana Agudelo<sup>1,2,3</sup> , Jhan Carlo Espinoza<sup>1</sup> , Clementine Junquas<sup>1,3</sup>, Paola A. Arias<sup>2</sup> , Juan Pablo Sierra<sup>1,4</sup> , and Matias E. Olmo<sup>5,6,7,8</sup> 

<sup>1</sup>Univ. Grenoble Alpes, IRD, CNRS, Grenoble INP, IGE, Grenoble, France, <sup>2</sup>Grupo de Ingeniería y Gestión Ambiental (GIGA), Escuela Ambiental, Facultad de Ingeniería, Universidad de Antioquia, Medellín, Colombia, <sup>3</sup>Servicio Nacional de Meteorología e Hidrología (SENAMHI), Lima, Perú, <sup>4</sup>LMD/IPSL, École Polytechnique, Institut Polytechnique de Paris, ENS, PSL Research University, Sorbonne Université, CNRS, Palaiseau, France, <sup>5</sup>National Council of Scientific and Technical Research (CONICET), Buenos Aires, Argentina, <sup>6</sup>Department of Atmospheric and Ocean Sciences, Faculty of Exact and Natural Sciences, University of Buenos Aires (DCAO-FCEN-UBA), Buenos Aires, Argentina, <sup>7</sup>Institut Franco-Argentin d'Estudes sur le Climat et ses Impacts (IFAECI IRL 3351/CNRS-IRD-CONICET-UBA), Buenos Aires, Argentina, <sup>8</sup>Barcelona Supercomputing Center, Barcelona, Spain

**Abstract** The last few decades have shown evidence of a lengthening dry season in southern Amazonia, which is associated with a delay in the onset of the South American Monsoon System (SAMS). Using a pattern recognition framework of atmospheric circulation patterns (CPs), previous studies have identified specific atmospheric situations related to the onset of the SAMS. Here, we analyze the future changes in the CPs that largely define the main hydro-climatological states of Tropical South America. We evaluated the CP changes that occurred between two periods: historical (1970–2000) and future (2040–2070), using six General Circulation Models (GCMs) from the Coupled Model Intercomparison Project Phase 6. Future GCM projections show significant spatio-temporal changes in the CPs associated with the dry season in southern Amazonia during the mid-21st century. These changes are related to both a late onset of the SAMS and an early demise of the SAMS. Particularly, the CP methodology allowed for a better understanding of the behavior of the southern Amazon dry season under future conditions, showing an increase in the frequency of the CPs typically observed during the dry season. The occurrence of dry days in the Amazon basin during the austral winter of the mid-21st century increases by 19.4% on average, with respect to the historical period. This methodology also identified a future increase in the frequency of dry CPs, both at the beginning of the dry-to-wet transition period (8%) and at the end of the wet-to-dry transition season (11%).

**Plain Language Summary** The southern Amazon has experienced a lengthening of the dry season over the past few decades. This trend has negative impacts on ecological services offered by the Amazon basin, affecting not only the region itself but also the entire planet. This is due to the fact that the Amazon basin plays a critical role in preserving the global hydrological and energy balance. We identify the future changes in the main atmospheric states in South Tropical South America, called atmospheric circulation patterns (CPs). These CPs can be interpreted as an average of each dominant meteorological situation over the region. For this purpose, we evaluated the projected changes occurring in the CPs considering two periods: historical (1970–2000) and future (2040–2070), using six global models. Our results show temporal and spatial variations in the CPs associated with the dry season during the mid-21st century. These changes are related to both a late dry season ending and an early dry season arrival. For the future period we detect an increase in the frequency of the CPs typically observed during the dry season (19% higher than historical period). This is particularly important in a region already threatened by land use and climate change.

## 1. Introduction

South Tropical South America (STSA) is defined as the region between 10°N–30°S and 90°W–30°W, including among other ecosystems, the tropical Andes and the Amazon Basin. This region hosts the largest water basin in the world and a dynamic ecosystem that covers areas of Brazil, Peru, Bolivia, Colombia, Ecuador, Venezuela, Guyana, and Suriname (Nobre et al., 2009). Thus, STSA is an important region for regional and global hydroclimatology due to the multiple interactions between biomes, land surface and atmospheric processes (Cai

et al., 2020; Marengo et al., 2018; Sousa et al., 2022). The South American Monsoon System (SAMS) is one of the key components in determining the regional climate dynamics, and a key driver of the rainy season in the region (Arias et al., 2015; Marengo et al., 2012; Orrison et al., 2022; Pascale et al., 2019; Vera et al., 2006; among others). Precipitation related to the SAMS mainly affects the central and southern part of the Amazon rainforest and the Cerrado biome, where the wet season is observed during the austral summer (e.g., Correa et al., 2021; Espinoza et al., 2009, 2020; Garreaud, 2009).

During the last decades, STSA, mainly southern Amazonia (around 5°–15°S and 70°–50°W) has experienced a lengthening of the dry season related with a delayed SAMS onset (Arias et al., 2015; Correa et al., 2021; Debortoli et al., 2015; Espinoza et al., 2019; Fu et al., 2013; Giráldez et al., 2020; Pascale et al., 2019). On the other hand, recent studies also show that delays of the SAMS onset are affected by anthropogenic forcing, including the influence of the forest-to-cropland conversion and deforestation (Butt et al., 2011; Debortoli et al., 2015; Ruiz-Vásquez et al., 2020; Sierra et al., 2023). These delays have been found to also be related to reduced cold front incursions in the Amazon basin, changes in the latitudinal location of the subtropical jet stream in the southern hemisphere (Fu et al., 2013), as well as inter-annual/decadal variability of the surface temperatures in the Pacific and Atlantic Oceans (Arias et al., 2015; Marengo et al., 2017).

Increases in the dry-day frequency, particularly during the September–October–November (SON) season, and the dry season length in the southern Amazon are related to alterations in the regional atmospheric circulation (Espinoza et al., 2019). Specifically, these increases are associated with changes in the continental Hadley cell, with enhanced subsidence over the central and southwestern Amazon during the long dry seasons (Arias et al., 2015; Espinoza et al., 2019; Marengo et al., 2022; Rao et al., 2022). The most recent assessment report of the Intergovernmental Panel on Climate Change (IPCC) indicates high confidence in a delayed onset of the SAMS (Douville et al., 2021), with associated modifications in the STSA hydrological cycle and atmospheric circulation, according to recent studies (Alves et al., 2017; Caballero et al., 2022; Costa & Pires, 2010; Marengo et al., 2018; Sierra et al., 2021; Silva et al., 2020; Wongchuig et al., 2022; Zilli & Carvalho, 2021). Changes in the main features of the atmospheric regimes during the dry and dry-to-wet transition season in STSA can provide additional information about the role of large-scale climate variability. This could provide new insights of the observed dry season lengthening over the region and its related impacts on variables such as atmospheric moisture transport, evaporation and precipitation regimes (Agudelo et al., 2019).

Using a pattern recognition framework of weather typing or atmospheric circulation patterns (CPs), Espinoza et al. (2021) investigate the daily atmospheric circulation regimes over STSA. CPs are usually defined as recurrent and potentially predictable atmospheric states, which can be related to dependent local variables such as rainfall or temperature (Bettolli et al., 2010; Hewitson & Crane, 2002; Moron et al., 2008; Solman & Menéndez, 2003). Applying this methodology, Espinoza et al. (2021) explain the occurrence of prolonged dry seasons in this region due to the higher frequency of a specific CP associated with enhanced subsidence over the southeastern Amazon basin. Likewise, a lower occurrence of a weather type characterized by wind intrusions from the south and convective activity over STSA is found by these authors in the SON season during the period 1979–2020. In contrast, CPs typically observed during the austral winter are more frequent during SON in the last decades.

General Circulation Models (GCMs) are important tools to better understand the physical mechanisms that determine present and projected climate changes over STSA, as a consequence of natural variability and/or anthropogenic radiative forcing (Almazroui et al., 2021; de Souza Costa et al., 2020; Ortega et al., 2021; Rivera & Arnould, 2020). The most recent and improved versions of these GCMs are included in the sixth phase of CMIP (CMIP6; Eyring et al., 2016). Some studies have shown that models such as CanESM5, IPSL-CM6A-LR, CESM2, MPI-ESM1-2-HR, and ACCESS-ESM1-5 have a better representation of different atmospheric variables in South America. Particularly, these GCMs have a better performance simulating precipitation and surface air temperature in regions like the Andes mountains, the Guianas, Mesoamerica, and the Cerrado region (Dias & Reboita, 2021; Monteverde et al., 2022). The latest generation of GCMs assembled under CMIP6 was found to represent the mean state of atmospheric variables better than previous versions introduced by CMIP5 (Fan et al., 2020; Li et al., 2021; Wainwright et al., 2021). In particular, Parsons (2020) used CMIP6 models to examine the shifting risk of eastern Amazonian droughts under high and low future greenhouse gas (GHG) emission scenarios. CMIP6 models suggest that global warming may be increasing the likelihood of exceptionally hot droughts in the region. With unabated global warming, anomalous warm and severe droughts will become more common by the mid-21st century. In addition, CMIP6 models agree on the sign of future rainfall trends in the Amazon better than the CMIP5 models (Parsons, 2020).

Olmo et al. (2022) focused on a process-based assessment to evaluate the performance of a set of historical simulations by 16 CMIP6 GCMs in reproducing the CPs and their associated rainfall over STSA, following Espinoza et al. (2021) weather-typing methodology. These authors identified the models with the best representation of CPs in this region. Particularly, these models are able to simulate the different atmospheric states represented by the CPs that characterize the main surface circulation in STSA, as well as their spatial and temporal variability. Thus, the authors selected some GCMs with the best representation of the main CP, including CPs related to the SAMS onset, with respect to observational and reanalysis data.

These studies suggest that using the CP approach can be an attractive methodology to evaluate the simulations from global and regional climate models, since atmospheric circulation is generally better represented by climate models than precipitation (Ban et al., 2021; Flato et al., 2013; Fossler et al., 2015; Kendon et al., 2012; Pichelli et al., 2021). In this regard, the main objective of the present study is to identify the projected changes in the regional low-level circulation in STSA under a regional rivalry climate change scenario. Thus, in this study we used the models identified by Olmo et al. (2022) with the best simulation of the CP dynamics over STSA. In order to identify future changes, we used model projections under the SSP3-7.0 scenario (Fujimori et al., 2017; Riahi et al., 2017). In particular, we focused on analyzing the CP changes in the dry season and the dry-to-wet transition season for the mid-21st century. For this purpose, we mainly focus on two types of analysis (a) changes in the frequency of CPs and (b) changes in their spatial patterns. This study aims to investigate whether the observed lengthening of the dry season in the STSA is also projected in future simulations of GCMs. Additionally, the study aims to explore the physical mechanisms associated with this process, particularly focusing on the regional low-level circulation.

This paper is organized as follows: Section 2 presents the data and methodology used in this study, the main results are detailed and analyzed in Section 3, and the summary and final remarks are provided in Section 4.

## 2. Data and Methodology

### 2.1. Reference Data Sets

#### 2.1.1. Atmospheric Data

The European Center for Medium-Range Weather Forecast (ECMWF) ERA5 reanalysis data set (Hersbach et al., 2020) was used to analyze the low-level atmospheric circulation from daily zonal and meridional wind over STSA (the region between 10°N and 30°S and 90°W–30°W) during the period 1970–2000. This period was chosen in order to obtain significant differences concerning the mid-21st century. Since the analysis of more recent periods was previously performed by Olmo et al. (2022) (1979–2014) and Espinoza et al. (2021) (1979–2020), this study considered to extend the time frame of analysis of atmospheric CPs over the STSA further into the past, assessing a historical period further away from the one analyzed in the previous studies.

In order to compare ERA5 data with the outputs from different selected GCMs, daily average data were bilinearly interpolated into a 1.0° × 1.0° grid resolution. ERA5 data sets are available online (<https://www.ecmwf.int/en/forecasts/datasets/reanalysis-datasets/era5>). In particular, we considered daily data for horizontal winds at 850 hPa to define the low-level CPs.

#### 2.1.2. Precipitation Data

The Climate Hazards Group Infrared Precipitation with Stations (CHIRPS) data set (Funk et al., 2014) was used as the precipitation reference to analyze rainfall variability and its relationship with the CPs over STSA. This precipitation product is obtained from satellite and rain gauge data and is available with a grid resolution of ~0.05° on a daily scale from 1981 to the present. In previous studies, CHIRPS has been evaluated and identified as a suitable dataset over STSA because it adequately represents precipitation variability in the region (e.g., Arias et al., 2020; Olmo & Bettoli, 2021; Segura et al., 2019). For this work, CHIRPS rainfall estimates were considered during the 1981–2000 period. Using bilinear interpolation these data were re-gridded into a 1.0° × 1.0° spatial resolution to be compared with the GCMs historical outputs. The CHIRPS v2.0 data set is available online ([https://data.chc.ucsb.edu/products/CHIRPS-2.0/global\\_daily/](https://data.chc.ucsb.edu/products/CHIRPS-2.0/global_daily/)).

### 2.2. General Circulation Models

In this study, we considered the same six GCMs selected by Olmo et al. (2022) shown in Table 1. Also, we followed the same approach based on a CP analysis (Espinoza et al., 2021). For this purpose, we considered

**Table 1**

*CMIP6 General Circulation Models (GCMs) Used in This Study for the Historical (1970–2000) and SSP3-7.0 (2040–2070) Simulations*

GCM	Horizontal resolution	Institute	Reference
ACCESS-ESM1-5	1.9° × 1.2°	Commonwealth Scientific and Industrial Research Organization (CSIRO), Australia	Ziehn et al. (2020)
CanESM5	2.8° × 2.8°	Canadian Center for Climate Modeling and Analysis, Canada	Swart et al. (2019)
CESM2	1.2° × 0.9°	National Center for Atmospheric Research (NCAR), USA	Danabasoglu et al. (2019)
IPSL-CM6A-LR	2.5° × 1.3°	Institut Pierre-Simon Laplace, France	Boucher et al. (2020)
MPI-ESM1-2-HR	0.9° × 0.9°	Max Planck Institute for Meteorology, Germany	Müller et al. (2018)
NorESM2-MM	0.9° × 1.2°	Norwegian Climate Center, Norway	Bentsen et al. (2013)

the daily zonal and meridional winds at 850 hPa over STSA (defined as the region between 10°N and 30°S and 90°W–30°W) during the period 1970–2000 for the historical experiment and the period 2040–2070 under the SSP3-7.0 scenario. This scenario was chosen considering it implies high challenges on both mitigation and adaptation, as a result of the combination of high GHG emissions and low mitigative capacity (Fujimori et al., 2017; Riahi et al., 2017). Only the r1i1p1f1 simulations were considered for both historical and future experiments. To compare historical simulations and future projections among the GCMs used, daily mean data were bilinearly interpolated on a 1.0° × 1.0° grid resolution. This approach facilitates model comparison through the use of a multimodel average. However, our primary focus was on individually analyzing the results for each model to avoid overlooking crucial details in the projected changes associated with the different atmospheric mechanisms. Furthermore, we estimated the annual cycle of the relative frequencies for the CPs, both using the original model resolution and the interpolated data. Then, no significant biases were identified in the categorization and frequency of CPs due to the resolution changes in each model (not shown). CMIP6 model outputs are available online through the Earth System Grid Federation (ESGF) CMIP data center (<https://esgf-node.llnl.gov/search/cmip6/>).

### 2.3. Dry Season Timing

This study focuses on the analysis of the dry season timing (arrival, ending and length) over the region between 5° and 15°S and 50°–70°W. To estimate the yearly dates of the dry season ending (DSE) and dry season arrival (DSA), we used the methodology developed by Li and Fu (2004). In order to reduce the synoptic noise, pentad rainfall time series are estimated by temporally averaging over a 5-day period, therefore, 1 year corresponds to 73 pentads. The DSE is established when six out of eight preceding pentads are below the climatological rain rate annual mean and six out of eight subsequent pentads are above it. Similarly, the DSA is established when six out of eight preceding pentads are above the climatological rain rate annual mean and six out of eight subsequent pentads are below it. Finally, the dry season length (DSL) is set as the number of pentads occurring between DSA and DSE dates (Fu et al., 2013). We evaluated the spatial homogeneity of the dry season arrival (DSA) and dry season end (DSE) dates within the predefined region and observed a high degree of uniformity for both dates across the study area (not shown).

### 2.4. Definition of Circulation Patterns

We used the methodology of the pattern recognition framework of weather typing or atmospheric circulation patterns (CPs) described by Espinoza et al. (2021) for STSA. Espinoza et al. (2021) identified and characterized nine CPs from the standardized anomalies of zonal and meridional winds at 850 hPa over the region 10°N–30°S, 90°W–30°W. Horizontal winds at 850 hPa have proven to be suitable for the description of the main low-level atmospheric circulation features in tropical South America (Paccini et al., 2018). Standardized wind anomalies were calculated using the long-term mean and standard deviation and then clustered without any time filter. This approach provides a large-scale overview of the atmospheric variability by considering, a priori, all time scales from daily to decadal, including long-term trends (Espinoza et al., 2021).

The low-level wind anomalies were synthesized using the Empirical Orthogonal Function (EOF) technique preserving at least 75% of the total variance of the data (Olmo et al., 2022). This ensures that the analysis focuses on the most dominant circulation phenomena, reducing the computational cost. This technique has been used in

previous studies to filter out the smallest spatial scales of the regional-scale atmosphere's phase space (Moron et al., 2008, 2015). Then, a cluster analysis was performed based on the subspace defined by the main EOFs using the *k*-means algorithm (Wilks, 2019). Note that in this study, whenever CPs are mentioned, we are specifically referring to atmospheric circulation patterns and not to Principal Component Analysis. A more exhaustive description of the atmospheric circulation patterns and associated mechanisms in STSA is discussed by Espinoza et al. (2021) and Olmo et al. (2022).

This methodology was applied to each GCM in order to obtain the simulated CPs for the historical period. The model CPs resulting from the cluster analysis were compared to those found in the ERA5 reanalysis. Following the procedure performed by Olmo et al. (2022), applying the minimum Euclidean distance criterion, model CPs during the historical period were matched to the reference ERA5 CPs by comparing their respective centroids. Finally, the same procedure was replicated for the future period. For the mid-21st century case, the simulated CPs from each GCM were compared to the ones identified in the historical period. Thus, future CPs were matched to the model CPs from the historical period, according to the criterion of minimum Euclidean distance between their respective centroids. It is important to highlight that the minimum Euclidean distance criterion allows for the consideration of not only the spatial distribution but also the magnitude of the studied variable. This criterion is particularly relevant for the classification of CPs, as it takes into account the significance of wind magnitudes.

The low-level horizontal wind and rainfall anomalies for each CP, according to the reference data described in Section 2.1 (ERA5 and CHIRPS, respectively), are shown in Figure 1. The precipitation anomalies were calculated based on the annual mean. This approach enables straightforward comparisons of the main rainfall structures characterizing each season and their transitions throughout the year. This analysis allows the identification of 9 CPs: 3 “winter” CPs (W1, W2, and W3), 3 “summer” CPs (S1, S2, and S3), and 3 “transitional” CPs (T1 and T2<sub>dw</sub> mostly for the dry-to-wet transition season and T3<sub>wd</sub> for the wet-to-dry transition season) (Espinoza et al., 2021). In general, summer CPs are associated with enhanced precipitation over STSA, with northerly low-level winds over the region. While S1 and S3 may exhibit similarities, these three CPs (S1, S2, and S3) represent distinct stages of the dominant modes of intraseasonal precipitation variability for the South Atlantic Convergence Zone (SACZ) and Southeastern South America (SESA) (Chug et al., 2022; Junquas et al., 2012). Indeed, S1 is more characteristic of convergence over the southern Amazon while S2 is over the SESA region. S3, however, is mostly associated with convergence over the continental SACZ and the Northeast of Brazil. In contrast, winter CPs are related to enhanced precipitation over North Tropical South America in association with stronger southerly winds. Although W1 and W3 may appear similar, these patterns are actually linked to different stages in the evolution of the South American Low-Level Jet (SALLJ). W3 corresponds to the mature phase of the winter SALLJ. It is characterized by stronger southward winds in the eastern Andes region (south of 1°S). In contrast, W1 corresponds to the initial phase of the winter SALLJ development, where this characteristic is not yet well established. More detail about the main features of the low-level atmospheric circulation associated with each CP is given in Olmo et al. (2022).

Using ERA5 reanalysis, previous studies defined CP using different periods 1979–2020 and 1979–2014 in Espinoza et al. (2021) and Olmo et al. (2022), respectively. These studies primarily focused on analyzing present-time periods. In the current study, we extended the analysis period to 1970–2000 to capture the historical behavior of the CPs, aiming to broaden the scope of CP study. However, no significant changes were found in the annual frequencies of CPs when comparing these three time periods (no shown).

### 3. Results

#### 3.1. Identification of Historical and Future Atmospheric CPs

The regional low-level atmospheric circulation variability is summarized through nine CPs that can be understood as preferred atmospheric states throughout the year (Figure 1). Figure 2 shows the relative mean daily frequency of the nine CPs in STSA as depicted by the ERA5 reanalysis and the six GCMs for historical and future simulations. As described by Espinoza et al. (2021) for observational datasets, the analyzed GCMs also show a clear seasonal cycle in the relative CPs frequency during the historical period (Figure 2). The annual cycles of the CPs simulated by each model for the mid-21st century show an increase in the frequencies of the winter CPs (W1, W2, and W3; in red-orange colors) during the southern Amazon dry season (Figure 2). For five out of the six GCMs studied (except CanESM5), the W1, W2, and W3 CPs appear earlier in the year (March, instead of

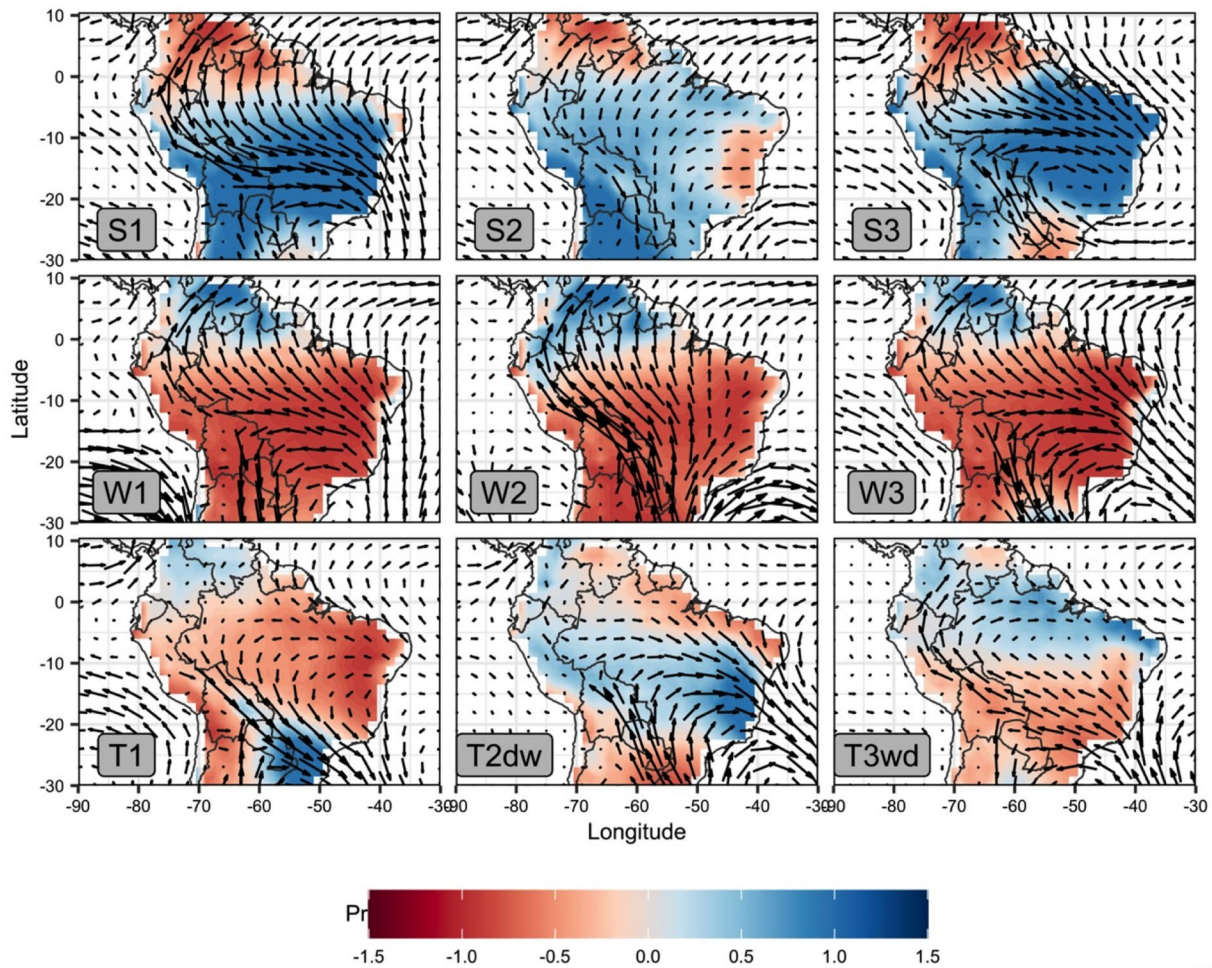


**Figure 1.** Spatial patterns of low-level wind and rainfall anomalies (in m/s and mm/day, respectively) for the nine circulation-patterns (CPs) in South Tropical South America, as depicted by the ERA5 reanalysis. Taken from Olmo et al. (2022). This analysis allows the identification of nine CPs: 3 “winter” CPs (W1, W2, and W3), 3 “summer” CPs (S1, S2, and S3) and 3 “transitional” CPs (T1 and T2<sub>dw</sub> mostly for the dry-to-wet transition season and T3<sub>wd</sub> for the wet-to-dry transition season). Vectors indicate wind anomalies at 850 hPa and shaded colors refer to CHIRPS rainfall anomalies.

April) and extend their occurrence until late November (instead of late October) in comparison to the historical simulations.

In the case of the CESM2 and MPI-ESM1-2-HR models, the applied methodology does not detect the atmospheric state represented by the S3 CP during the future period (Figure 2). Statistically, this is explained by a decrease in the atmospheric variability during summertime in these simulations. According to Figure S1 in Supporting Information S1, over STSA, the variance for the U-wind component decreases from 4.1 m/s to 3.6 m/s during summertime (DJF), when moving from the historical to the future period for the CESM2 model (reduction of 0.5 m/s). In the MPI-ESM1-2-HR model, this projected reduction averages 0.6 m/s (estimated values of 3.5 m/s and 2.9 m/s for the historical and future periods, respectively). These values were obtained by spatially averaging the U-wind variance fields considering the entire STSA region (10°N–30°S and 90°W–30°W) for both periods (historical and future). The *k*-means method is based on the minimization of within-cluster (within-CPs) 850 hPa wind variances. Therefore, the methodology does not capture the three summer CPs identified in the historical simulation of these models, and an optimal clustering is found with two summer CPs. In contrast, a fourth winter CP is detected in these GCMs in the future simulations (Figure 2). See the spatial pattern in Figure S2 in Supporting Information S1). Based on the predetermined condition, the method is designed to identify nine CPs. However, in the case of the CESM2 and MPI-ESM1-2-HR models, an additional CP is identified during winter, while one CP is missing during summer. This discrepancy arises from the variance of the winds, which

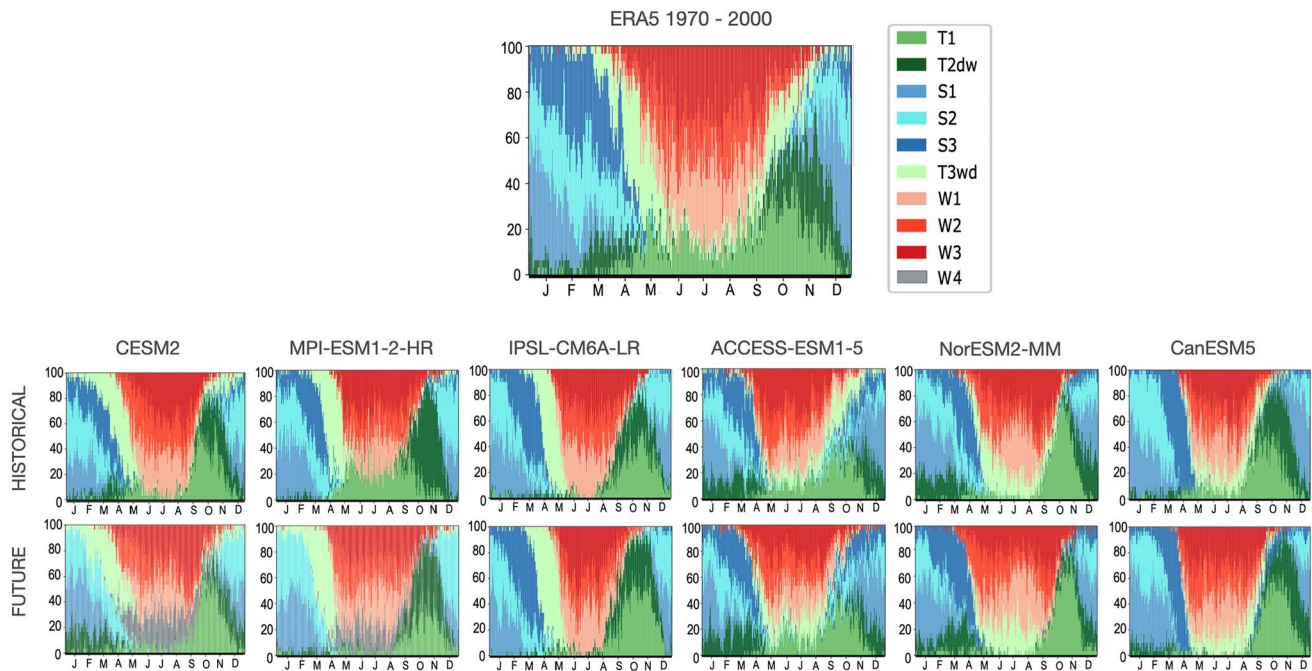


**Figure 2.** Relative mean daily frequency of the nine CPs in STSA as depicted by the ERA5 reanalysis and six GCMs for historical and future simulations. The x-axis displays the 365 days of the year, while the y-axis indicates the relative mean daily frequency of each CP. The annual frequency cycle for ERA5 has been calculated for the representative years of the historical period (1970–2000).

increases in winter and decreases in summer, as depicted in Figure S1 in Supporting Information S1. Notably, the newly identified CP, W4, emerges at the onset of winter in the CESM2 model and at a later time in the MPI model (Figure 2). This variation in timing explains the differences observed in the W4 patterns obtained for these two models.

In addition, the ACCESS-ESM1-5, NorESM2-MM, and CanESM5 models no longer exhibit T3<sub>wd</sub> as the CP that marks the wet-to-dry transition, according to their future simulations. In the future period, this CP has a wider range of occurrence during the dry season, being a drier CP compared to its main features during the historical period (see Figure S3 in Supporting Information S1).

### 3.2. Changes in Circulation Patterns and Associated Rainfall

For a deeper insight on the models' ability to adequately simulate the CPs and its projections according to the selected future scenario, this section shows the spatial patterns of the 850 hPa wind and rainfall anomalies for some representative CPs during the transition, summer, and winter time. Figure 3 shows the spatial pattern of T2<sub>dw</sub>. This CP represents the onset of the SAMS (i.e., the DSE), characterized by wind convergence over the southern Amazon and the SACZ region and southerly wind intrusion reaching the southern Amazon, related to a cyclonic circulation over the south tropical Atlantic Ocean. The third column of Figure 3 shows the significant projected changes for this CP.

The projected changes for the multimodel average (Figure 3c) show an intensification of the anomalous northerly cross-equatorial wind, stronger wind convergence over the southern Amazon and SACZ, and increased humidity in central Amazonia and the Andes. Besides, it also leads to negative precipitation changes over the northern region of South America and positive anomalies over the southeastern Amazon. However, these multimodel projected changes are strongly dominated by features of wind circulation and convergence from the CESM2 model. For the rest of the models, we can see a projected drier transition from the dry-to-wet season over the southeastern Amazon region. A weakening of the northerly cross-equatorial winds is also projected, which may block the atmospheric moisture transport from the Caribbean to the SACZ region, contributing to a drier southeastern Amazon. Particularly, models such as MPI-ESM1-2-HR, ACCESS-ESM1-5, and

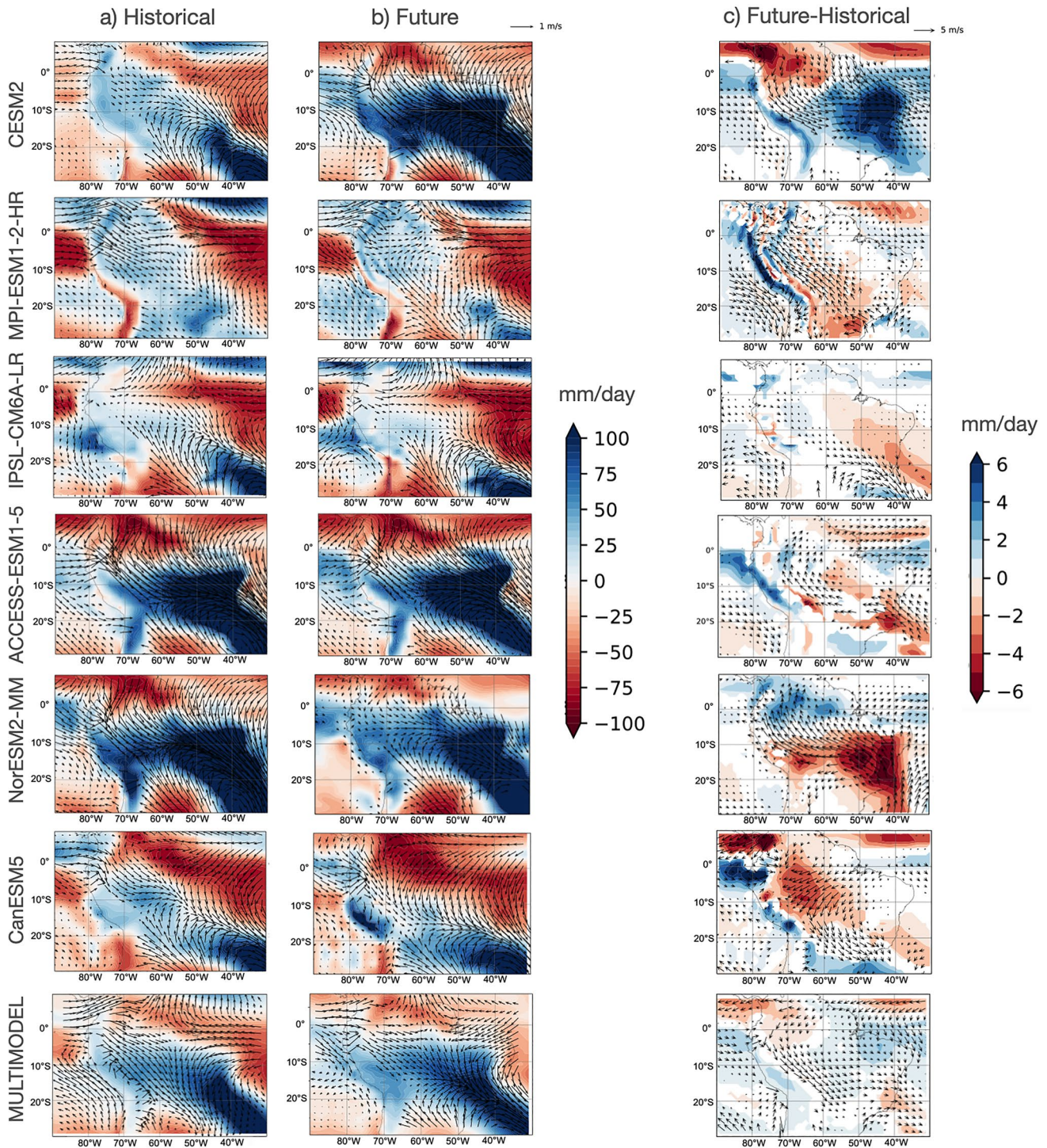


**Figure 3.** Spatial patterns of 850 hPa wind and rainfall anomalies for the  $T2_{dw}$  CP, which represents the onset of the SAMS, for (a) the historical period (1970–2000), (b) the future period (2040–2070) and (c) the changes between both periods (future-historical). Vectors indicate wind anomalies at 850 hPa and shaded colors refer to rainfall anomalies in mm/day. The third column displays the significant changes in precipitation (shades) and wind (vectors) according to a  $t$ -test ( $p < 0.05$ ).

NorESM2-MM clearly show a reduction in low-level convergence for the future scenario, displaying negative precipitation anomalies over the same region. In particular, a further decrease in low-level winds convergence is projected over the southeastern Amazon, probably contributing to the delay of the wet season onset in this region.



The MPI-ESM1-2-HR, NorESM2-MM, and CanESM5 models show a reduction of precipitation over southeastern South America (SESA) region due to the decrease of southerly winds coming from the La Plata Basin, which are part of the cyclonic circulation over the south tropical Atlantic Ocean.

In general, it is evident that the models face challenges in adequately representing CP T2wd, resulting in significant biases when compared to the T2wd shown in Figure 1. As explained in Olmo et al. (2022), models tended to have more difficulties in simulating the frequencies of transitional CPs, especially T1 and T2<sub>dw</sub>. Specifically, for the MPI-ESM1-2-HR model, T2wd proves to be the most difficult to accurately represent (Figure 3 in Olmo et al., 2022).

Figures 4 and 5 illustrate the spatial patterns of S1 and W2, respectively. S1 represents the mature phase of the SAMS characterized by wet conditions, while W2 represents the winter conditions preceding the onset of SAMS, characterized by dry conditions. Figures 4 and 5 display the spatial patterns for the six CMIP6 models along with their multimodel average.

In the changes projected in Figure 4 for the multimodel mean, a weakening of the cyclonic circulation over the west Atlantic subtropical coast is detected, which is a prominent characteristic of this CP. Consequently, there is a decrease in the convergence of low-level winds over the SACZ region. It is important to highlight that this result is heavily influenced by the projected changes in the CESM2 model (Figure 4c). Additionally, the future period shows a less pronounced intrusion of southerly winds over the La Plata basin. In terms of precipitation changes, a reduction is projected for the southeastern Amazon, while an increase is anticipated in northern South America.

The mid-21st century projections of S1 show that the southerly wind intrusion from La Plata basin to the Amazon is projected to be more intense (weaker) in the MPI-ESM1-2-HR and ACCESS-ESM1-5 (CESM2 and NorESM2-MM) models. For the CESM2 model, the cyclonic circulation over the Atlantic coast is projected to weaken by the mid-21st century. The wind anomalies corresponding to the differences between the two periods show an anticyclonic circulation over the southeastern Amazon. Consequently, precipitation anomalies show a decrease (increase) in rainfall over the eastern Amazon basin (SESA region).

For the S1 pattern, the ACCESS-ESM1-5 and NorESM2-MM models show a STSA region with less precipitation than the rest of the models for both periods (columns a and b in Figure 4). When focused on the estimated significant changes between the future and historical periods for the NorESM2-MM model, a significant decrease in precipitation is noted over a large area of the Amazon basin, particularly in the central and eastern regions. In contrast, the CESM2, MPI-ESM1-2-HR, ACCESS-ESM1-5 and CanESM5 models show positive precipitation anomalies over the Andes Mountains range under the SSP3-7.0 scenario by the mid-21st century.

Figure 5 shows the spatial patterns of precipitation and 850 hPa wind anomalies for the W2 pattern, which presents its major frequency during the core of the dry season (JJA). This particular CP presents a strong meridional component of the wind characterized by cold-surge intrusions into STSA coming from the La Plata basin, being the most sensitive CP to the representation of the meridional wind. The low-level circulation associated to this pattern is well-reproduced by the 6 selected GCMs, particularly the southerly cross-equatorial wind anomalies extended from the Bolivian Amazon to SESA and to the east of the Andes. Also, negative rainfall anomalies over the entire STSA are well simulated by all models as well as positive rainfall anomalies in the northern South American region.

The multimodel mean for CP W2 shows a decrease in the intensity of the southerly wind anomalies, particularly in the eastern region of the Andes (Figure 5c). This weakening of the cold-surge intrusions associated with this CP restricts their penetration further into the tropics. Consequently, this leads to drier conditions in northern South America while promoting wetter conditions in the western Amazon. The estimated significant changes between the future and historical periods for this CP show a decrease in the southerly winds over the SESA region for the MPI-ESM1-2-HR, IPSL-CM6A-LR, NorESM2-MM, and CanESM5 models, showing negative (positive) rainfall anomalies over the southern tropical Atlantic coast (SESA). Also, Figure 5c shows a decrease in the southerly cross-equatorial wind anomalies for CESM2, MPI-ESM1-2-HR, ACCESS-ESM1-5, and NorESM2-MM model for the future period. Consequently, a wetter western Amazon is projected as well as a clear and significant reduction of precipitation in northern South America.

It is important to highlight that all the models (except NorESM2-MM) show positive precipitation anomalies over the northern part of the Andes Mountains range under the SSP3-7.0 scenario by the mid-21st century, which agrees with previous studies (Ortega et al., 2021; Parsons, 2020).

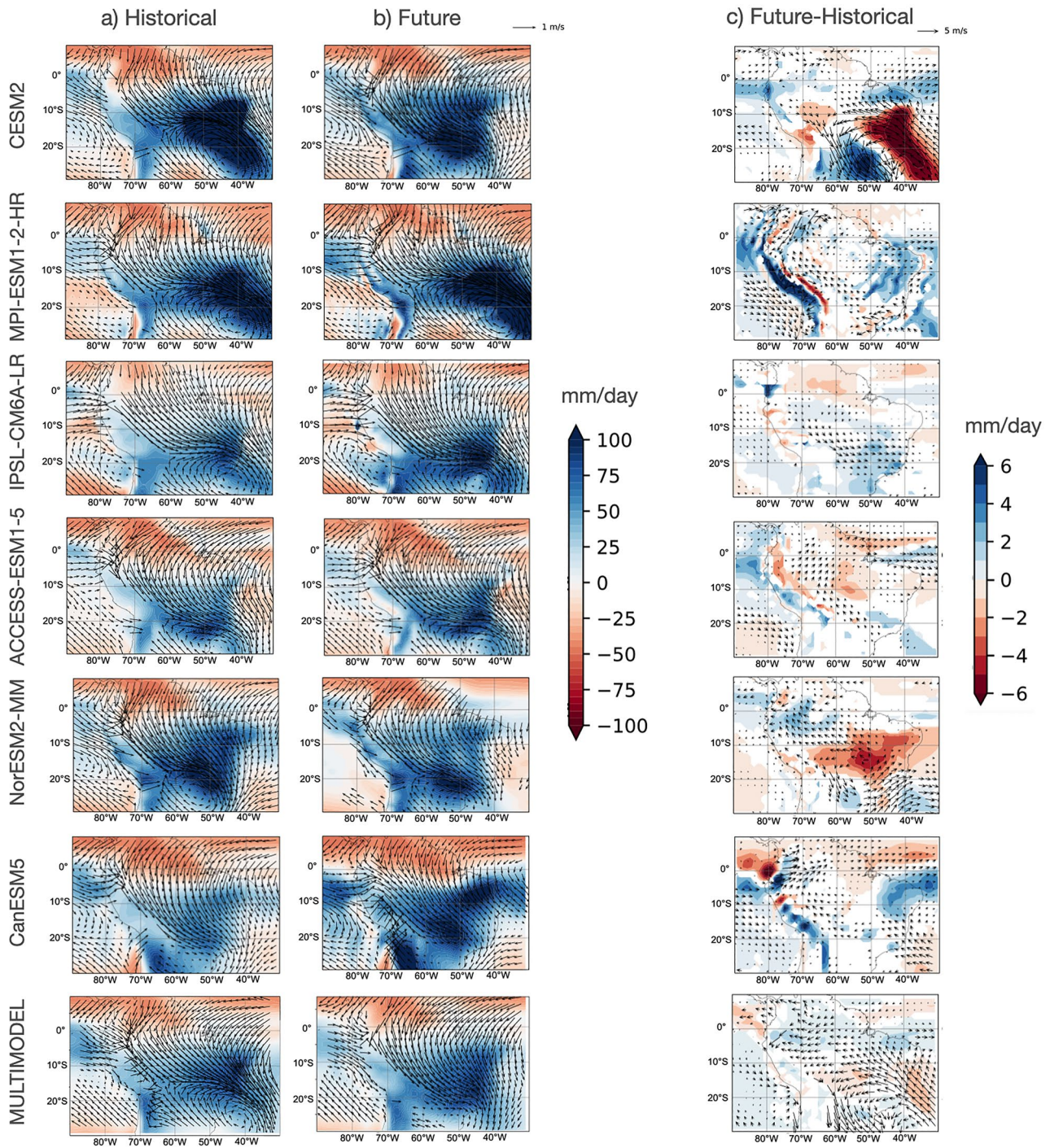


**Figure 4.** Spatial patterns of 850 hPa wind and rainfall anomalies for the S1 CP, which represents the SAMS mature phase during the austral summer, for (a) historical period (1970–2000), (b) future period (2040–2070) and (c) the difference between both periods (future–historical). Vectors indicate wind anomalies at 850 hPa and shaded colors refer to rainfall anomalies in mm/day. The third column displays the significant changes in precipitation (shades) and wind (vectors) according to a  $t$ -test ( $p < 0.05$ ).

### 3.3. The Future Dry Season Lengthening From CPs

To understand how CPs may change under the SSP3-7.0 scenario, Figure 6 shows the relative mean frequency of the CPs with significant changes during the mid-21st century, corresponding to two winter (W2 and W3) and two transition (T1 and T2<sub>dw</sub>) CPs, for both historical and future simulations. These particular CPs were selected

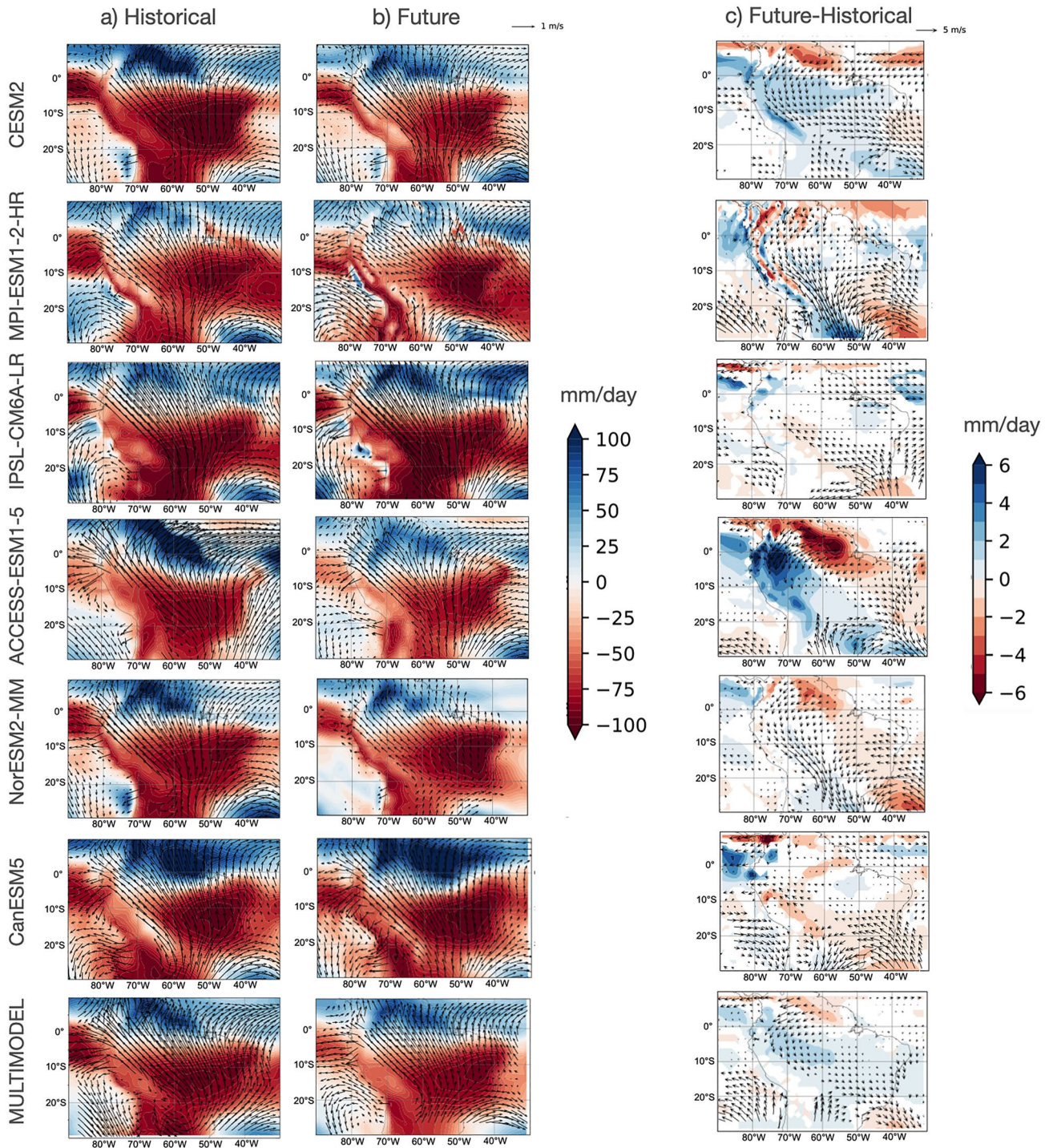


**Figure 5.** Spatial patterns of 850 hPa wind and rainfall anomalies for CP W2, which represents the winter conditions that precede the South American Monsoon System (SAMS) onset (i.e., DSE), for (a) historical period (1970–2000), (b) future period (2040–2070), and (c) the difference between both periods (future-historical). Vectors indicate wind anomalies at 850 hPa and shaded colors refer to rainfall anomalies in mm/day. The third column displays the significant changes in precipitation (shades) and wind (vectors) according to a  $t$ -test ( $p < 0.05$ ).

due to their relevance during the occurrence of dry season (Espinoza et al., 2021). W2 and W3 as indicators of the dry period, can offer valuable information about the length of the dry season. Conversely, T1 and T2 are associated with the onset of the monsoon, signifying the beginning of the rainy season (i.e., the DSE).

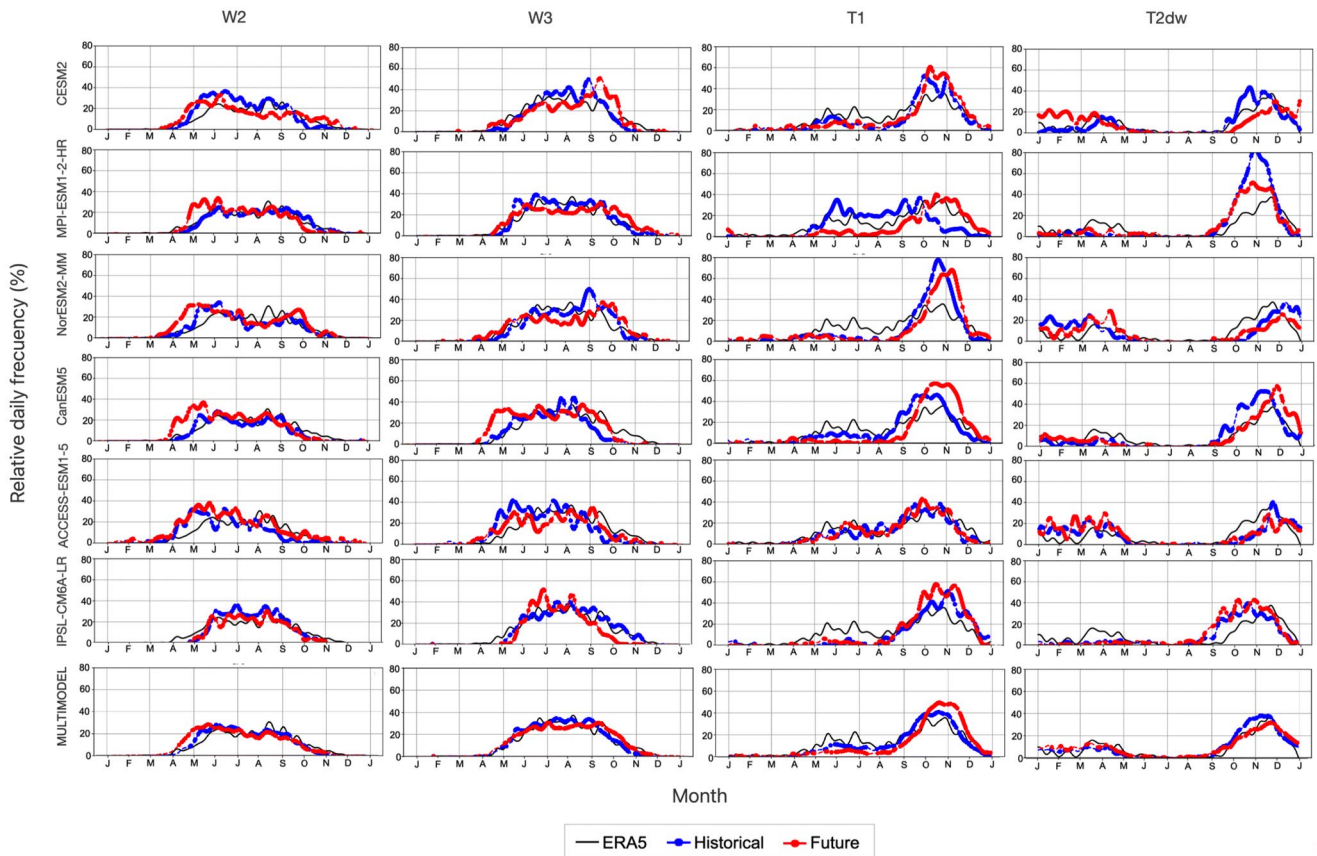


**Figure 6.** Relative mean daily frequency of winter (W2, W3) and transitional (T1 and T2<sub>dw</sub>) circulation patterns (CPs) defined from the *k*-means clustering analysis for the 6 GCMs selected during historical and future periods (blue and red lines, respectively). The reference line given by ERA5 for the same years of the historical period (1970–2000) is presented in black. The *x*-axis displays the 365 days of the year, while the *y*-axis indicates the relative mean daily frequency of each CP. Days with significant differences between historical and future periods are highlighted with red dots (*p*-value <0.05). Days with significant differences between observations and historical period are highlighted with blue dots (*p*-value <0.05). CPs annual cycles were smoothed using a temporal lowpass Butterworth filter, retaining only frequencies lower than 1/30 cycles per day.

The projected W2 CP shows increased frequencies during April, May, and June in comparison to the historical simulation for the CESM2, MPI-ESM1-2-HR, NorESM2-MM and CanESM5 models (left column in Figure 6). This suggests a higher frequency of days with drier conditions at the beginning of the dry season (between 10% and 20%), which may favor a more abrupt wet-to-dry transition in this region. The projected W3 CP exhibits increased frequencies by the end of the year for all the GCMs considered, excluding the IPSL-CM6A-LR model (Figure 6). Specifically, this CP, associated with dry conditions, occurs not only during the winter but also during October and November season (dry-to-wet transition), which could favor a late onset of the SAMS, and therefore a delayed DSE.

As discussed by Espinoza et al. (2021), the dry-to-wet transition period is largely dominated by the occurrence of the T1 and T2<sub>dw</sub> CPs. When comparing the mean annual cycle of the CP relative frequencies, it is noted that both T1 and T2<sub>dw</sub> CPs exhibit a slight delay in the time of their appearance during the months of September and October for the future period compared to the historical simulation (blue line in Figure 6) for CESM2, MPI-ESM1-2-HR, NorESM2-MM, and CanESM5 models. This is consistent with a later-than-usual DSE, which favors a delayed onset of the SAMS and consequently a delay in the onset of the rainy season in the southern Amazon region.

It should be noted that significant biases exist, particularly for CP T2<sub>dw</sub>, during the historical period. As explained by Olmo et al. (2022), the models encountered challenges in accurately simulating the frequencies of transition CPs, specifically T1 and T2<sub>dw</sub>. This outcome is partly expected considering that the definition of CPs is primarily driven by the seasonal cycle.

Finally, the ACCESS-ESM1-5 and IPSL-CM6A-LR models show no major changes in the relative mean daily frequencies of the PCs analyzed here.

When considering the results obtained for the multimodel average (last row of Figure 6), it is evident that the information aligns with the general behavior described by the six models considered, albeit at the cost of losing the individual details provided by each model. The multimodel average reveals an earlier occurrence of W2 in the future period. Moreover, a slight increase is detected for W3 during October–November. However, it is important to note that the results of the IPSL-CM6A-LR model disrupt the trend that is strongly observed in the remaining five models. Finally, in the multimodel average, CPs T1 and  $T_{2_{dw}}$  exhibit a slight delay in their timing during the future period. Differences of relative mean daily frequency between the historical and future periods can be seen in Figure S4 in Supporting Information S1.

### 3.4. Future Changes in Precipitation Annual Cycle and Dry Season Length

Figure 7 illustrates the climatological annual cycle of precipitation over the Southern Amazon region simulated by each GCM considered during the historical and future periods. The ACCESS-ESM1-5 and MPI-ESM1-2-HR models have the best representation of the precipitation annual cycle during the historical period (blue line) in comparison to CHIRPS (gray line). Models such as CanESM5, CESM2, and NorESM2-MM underestimate rainfall during the dry season (i.e., austral winter: June–July–August: JJA) and the transition to the wet season (SON) for the historical period, in agreement with Olmo et al. (2022). The IPSL-CM6A-LR model (Figure 7d) manages to adequately simulate precipitation during the dry season. Particularly, this model significantly underestimates precipitation during the austral summer (December–January–February: DJF). This model also shows the smallest change in the precipitation annual cycle between the historical and future periods. With the exception of the IPSL-CM6A-LR model, the remaining GCMs show a reduction of precipitation during the dry-to-wet transition season (SON) for future projections (red line), which is in agreement with the multimodel mean (Figure 7g).

The climatological pentad of occurrence of the DSA and DSE are shown in Table 2 (column 1 and 2, respectively), as well as in Figure 7 as dot markers. In addition, the climatological length of the dry season is presented in the third column of Table 2 for both historical and future periods. For reference, in the case of CHIRPS data, the DSA and DSE dates occur during pentads 19 and 60, respectively. This suggests that, on average, the dry season spans from April 5th to October 27th for this reference data set.

All the models show a projected increase of the DSL and a delayed DSE by the mid-21st century, but no agreement is found concerning the projected change of the DSA. This DSL increase is due to a delayed DSE (between 1 and three pentads, i.e., 5 and 15 days, all-model agreement) and a slightly earlier DSA (between 1 and two pentads earlier, i.e., 5 and 10 days, four of six models). For the DSA, the CESM2 model shows no change in the mean date of the dry season onset, while the IPSL-CM6A-LR model projects a late dry season onset. On the contrary, future projections show an early DSA, between 1 and two pentads, for the remaining models. The projected earlier DSA is statistically significant for the ACCESS-ESM1-5 and IPSL-CM6A-LR models (Table 2). In the case of the ACCESS-ESM1-5 model, the dry season is lengthened by four pentads, that is, 20 days, for the mid-21st century under the SSP3-7.0 scenario. This model presents the greatest changes in both DSA (10-day early onset) and DSE dates (10-day delayed end). For the CESM2, MPI-ESM1-2-HR, IPSL-CM6A-LR, and NorESM2-MM models, the DSL is projected to increase between 1 and two pentads, that is, 5 and 10 days.

Figure S5 in Supporting Information S1 shows that the six GCMs considered in this study exhibit an increasing trend in both DSL and DSE, becoming much stronger during the future period. The models show a unanimous positive trend for both DSL and DSE (about 0.96 pentad/decade and 0.8 pentad/decade on average, respectively). Table S1 in Supporting Information S1 shows linear trends, confidence intervals, and significance of the DSL and DSE dates for the periods 1970–2000 and 2040–2070.

The projected changes of dry season length documented in this section can be associated with changes in the mechanisms that govern the wet and dry seasons explained by changes in CPs (Sections 3.2 and 3.3). Specifically, this study projects a decrease in the convergence of low-level winds over the SACZ region and a weakening of the northerly cross-equatorial flow (Figure 4c). This results in reduced moisture transport from the tropical Atlantic Ocean to the continent, leading to drier conditions in the southeastern Amazon region (Figure 4c). In CP  $T_{2_{dw}}$ , there is no unanimous agreement among the models regarding the strengthening or weakening of the northerly cross-equatorial winds (Figure 3c). However, the majority of models (five out of six) suggest a decrease in rainfall

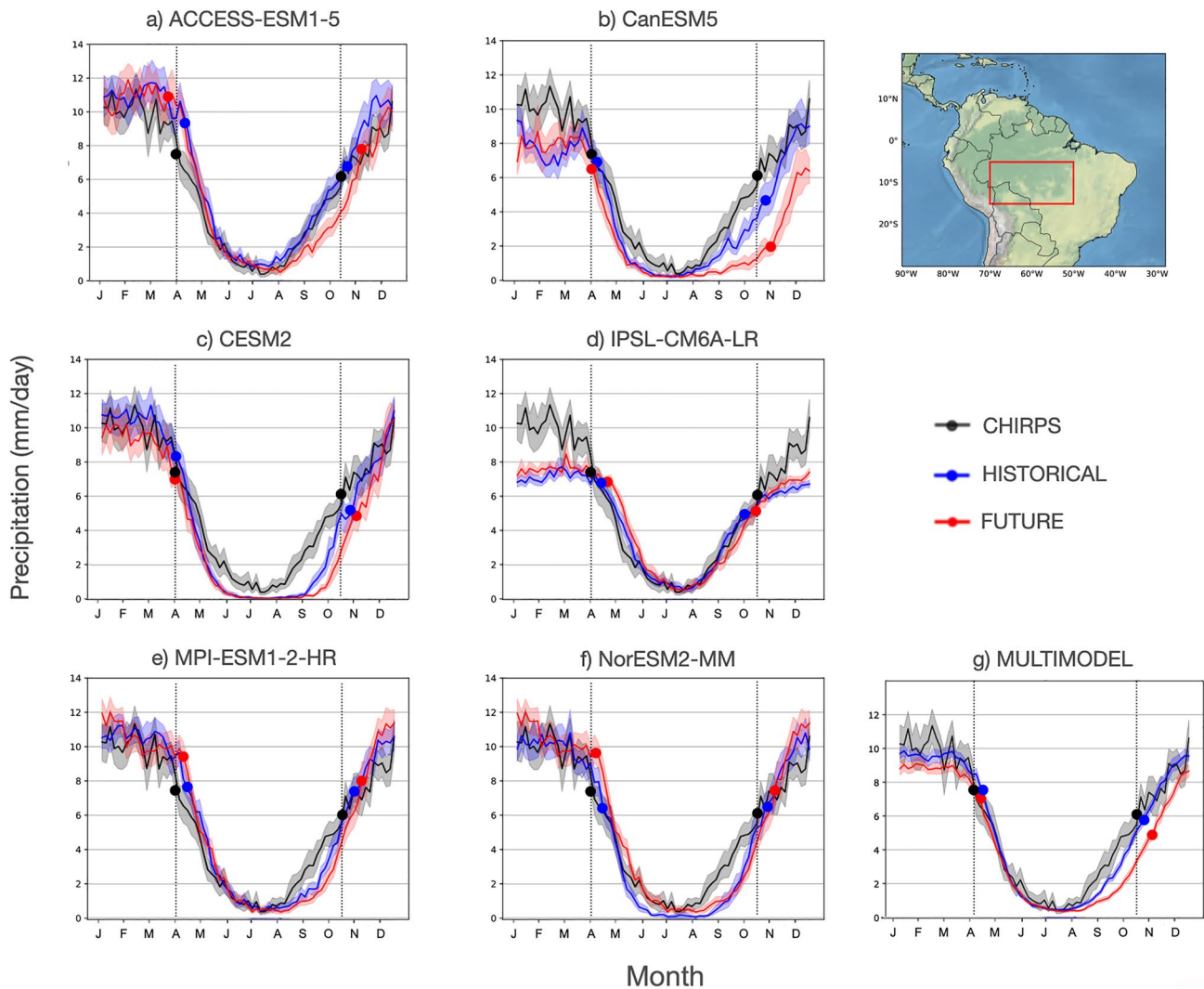


**Figure 7.** Precipitation annual cycles over southern Amazonia (domain between  $5^{\circ}$ – $15^{\circ}$ S and  $50^{\circ}$ – $70^{\circ}$ W), expressed in mm/day and smoothed using a 5-day moving window (pentad). The gray line indicates the CHIRPS reference data set during 1981–2000, and the blue (red) line indicates the climatological annual cycle simulated for the historical (future) period by the different GCMs: (a) ACCESS-ESM1-5, (b) CanESM5, (c) CESM2, (d) IPSL-CM6A-LR, (e) MPI-ESM1-HR, (f) NorESM2-MM, and (g) multimodel mean. The shadows show the envelope of uncertainty using bootstrapping. The confidence interval is constructed by taking a percentile interval of the bootstrap distribution. In this case, we draw a 95% confidence interval. The climatological dates of the dry season arrival (DSA) and dry season ending (DSE) are highlighted with circles.

for the western and southern Amazon basin during the future period (Figure 3c). Furthermore, a weakening of cold-surge intrusions associated with W2 is observed, concentrating the moisture transported by the southerly winds mostly in the eastern region of the Andes (Figure 5c). As a consequence, the southeastern Amazon experiences drier conditions during the future period (Figure 5c). These results suggest an anticipated delay in the occurrence of CP  $T_{2_{dw}}$ , which subsequently postpones the onset of the SAMS and prolongs the duration of the dry season (DSL) for the 2040–2070 period.

#### 4. Summary and Final Remarks

The occurrence of a longer dry season in the southern Amazon has been identified in multiple studies using different reference datasets (Agudelo et al., 2019; Arias et al., 2015; Correa et al., 2021; Debortoli et al., 2015; Fu et al., 2013). Moreover, future projections of an extended dry season in Amazonia have been addressed in previous studies (Boisier et al., 2015; Fu et al., 2013; Parsons, 2020). However, few of these studies discuss the atmospheric mechanisms associated with this fundamental change in the hydroclimate of this region. Therefore, this

**Table 2**  
Changes in DSA, DSE, and DSL Between the Future and Historical Periods (Number of Pentads) and Their Standard Deviation

	DSA		DSE		DSL	
	1970–2000	2040–2070	1970–2000	2040–2070	1970–2000	2040–2070
ACCESS-ESM1-5	20 ± 1.7	−2 ± 1.6	61 ± 2.1	+2 ± 1.7	41 ± 3.2	+4 ± 2.8
CanESM5	20 ± 1.1	−1 ± 1.4	62 ± 0.7	+1 ± 1.7	42 ± 0.9	+2 ± 2.1
CESM2	19 ± 1.9	0 ± 2.1	62 ± 0.8	+1 ± 1.4	43 ± 1.1	+1 ± 2.5
IPSL-CM6A-LR	22 ± 1.7	+1 ± 1.1	57 ± 2.0	+3 ± 2.1	35 ± 2.4	+1 ± 2.6
MPI-ESM1-2-HR	21 ± 1.8	−1 ± 2.0	62 ± 1.8	+1 ± 1.6	41 ± 2.3	+2 ± 2.5
NorESM2-MM	21 ± 1.7	−1 ± 2.2	62 ± 1.8	+1 ± 1.9	41 ± 2.8	+2 ± 2.8
MULTIMODEL	21 ± 1.2	−1 ± 1.8	62 ± 0.9	+1 ± 1.6	41 ± 2.4	+2 ± 2.1
CHIRPS (1981–2000)	19 (April 5) ± 1.7		60 (October 27) ± 1.2			

Note. The gray color indicates statistically significant changes according to a *t*-test ( $p < 0.05$ ). The dry season length (DSL) corresponds to the difference between DSE and DSA.

study focused on determining the possible future changes in the main low-level atmospheric circulation patterns related to the onset of the South American Monsoon System (SAMS) and therefore the dry season ending over the Amazon during the 2040–2070 period.

To do so, this study described and analyzed the main large-scale low-level atmospheric circulation patterns (CPs) in South Tropical South America (STSA) for two periods: 1970–2000 and 2040–2070, representing a historical and a future period, respectively. Nine CPs were defined based on a *k*-means clustering of low-level wind anomalies, considering the daily ERA5 atmospheric circulation and CHIRPS rainfall data as reference and using the weather-typing approach proposed by Espinoza et al. (2021). We built on the work by Olmo et al. (2022), who identified the models with the best representation of the regional low-level atmospheric circulation during the historical period. The six models with the best simulation of the CPs in STSA were considered in this study to estimate the projected changes under the SSP3-7.0 scenario by the mid-21st century (2040–2070).

This study primarily focuses on two types of analyses: (a) changes in the frequency of CPs, and (b) changes in their spatial patterns. Our results indicate a projected increase in the frequency of the CPS typically observed during the Amazon dry season by the mid-21st century. In addition, we identified a future increase in the frequency of dry CPs, both at the beginning of the dry-to-wet transition period and at the end of the wet-to-dry transition season. The changes in these CPs are associated with a reduction of convergence over the South Atlantic Convergence Zone (SACZ), which seems to be an important component in the future delay of the wet season in the southeastern Amazon.

This could help to explain the atmospheric mechanisms associated to the occurrence of drier conditions during the dry and transition seasons in the southern Amazon, contributing to a longer dry season in this region (Parsons, 2020). Our results show that the projected drier conditions over southeastern Amazonia and the continental part of the SACZ during the dry-to-wet transition season in STSA are related to a higher frequency of two winter CPs (W2 and W3), associated with dry conditions. Also, a lower frequency of one dry-to-wet transition CP ( $T_{2,dw}$ ), at the end of the dry season was projected by the mid-21st century. This could be associated with atmospheric changes contributing to a delayed DSE during the future period. These changes in the low-level atmospheric circulation have been associated with an enhanced Hadley circulation, which intensifies the atmospheric subsidence (rising motion) over STSA (northern South America) (e.g., Agudelo et al., 2019; Arias et al., 2015; Espinoza et al., 2019, 2021; Rao et al., 2022).

The results discussed here suggest that the low-level circulation is important for understanding whether GCMs can simulate the spatial and temporal climate variability over the STSA region. In addition, the CPs obtained from the low-level circulation include the major atmospheric patterns over STSA and can help organize larger scale structures for a global understanding of atmospheric processes, even in the middle and upper troposphere (Espinoza et al., 2021; Olmo et al., 2022).

It is important to highlight that our study reduces uncertainty in terms of the estimation of the future dry season onset and demise in the southern Amazon because: (a) we only used models that have a good representation of the mechanisms associated with the onset of the dry season, and (b) we explored the mechanisms associated with the lengthening of the dry season following a CP approach, based on the analyses of the low-level circulation in the region, which is generally better simulated by GCMs in comparison to precipitation. Considering the anticipated increase in drier conditions in STSA (Boisier et al., 2015; Cook et al., 2020; Moon & Ha, 2020; Parsons, 2020; Sena & Magnusdottir, 2020) and the potential impacts of deforestation on the regional precipitation cycle (Eiras-Barca et al., 2020; Ruiz-Vasquez et al., 2020; Sierra et al., 2021, 2023; Staal et al., 2018), further studies on this topic are highly relevant. It is crucial to comprehend the potential influence of a delayed wet season onset in the southern Amazon on rainfall patterns in nearby regions.

### Conflict of Interest

The authors declare no conflicts of interest relevant to this study.

### Data Availability Statement

The different data sets used in this study are available online. ERA5 reanalysis [Dataset] (Hersbach et al., 2020): <https://www.ecmwf.int/en/forecasts/datasets/reanalysis-datasets/era5>. CHIRPS V2.0 [Dataset] (Funk et al., 2014): [https://data.chc.ucsb.edu/products/CHIRPS-2.0/global\\_daily/](https://data.chc.ucsb.edu/products/CHIRPS-2.0/global_daily/). CMIP6 model outputs: <https://esgf-node.llnl.gov/search/cmip6/>.

### Acknowledgments

This work has been funded by the Water Cycle and Climate Change project (CECC; IRD/AFD) and by the French AMANECER-MOPGA project funded by ANR and IRD (Ref. ANR-18MPGA-0008). J.-C. Espinoza received support from Project 077-2021-FONDECYT (PROCIENCIA). Paola A. Arias was supported by MINCIENCIAS through Grant 20230017-25-2020.

### References

- Agudelo, J., Arias, P. A., Vieira, S. C., & Martínez, J. A. (2019). Influence of longer dry seasons in the Southern Amazon on patterns of water vapor transport over northern South America and the Caribbean. *Climate Dynamics*, 52(5), 2647–2665. <https://doi.org/10.1007/s00382-018-4285-1>
- Almazroui, M., Ashfaq, M., Islam, M. N., Rashid, I. U., Kamil, S., Abid, M. A., et al. (2021). Assessment of CMIP6 performance and projected temperature and precipitation changes over South America. *Earth Systems and Environment*, 5(2), 155–183. <https://doi.org/10.1007/s41748-021-00233-6>
- Alves, L. M., Marengo, J. A., Fu, R., & Bombardi, R. J. (2017). Sensitivity of Amazon regional climate to deforestation. *American Journal of Climate Change*, 6(1), 75–98. <https://doi.org/10.4236/ajcc.2017.61005>
- Arias, P. A., Fu, R., Vera, C. S., & Rojas, M. (2015). A correlated shortening of the North and South American monsoon seasons in the past few decades. *Climate Dynamics*, 45(11–12), 3183–3203. <https://doi.org/10.1007/s00382-015-2533-1>
- Arias, P. A., Martínez, J. A., Mejía, J. D., Pazos, M. J., Espinoza, J. C., & Wongchuig-Correa, S. (2020). Changes in normalized difference vegetation index in the Orinoco and Amazon River basins: Links to tropical Atlantic surface temperatures. *Journal of Climate*, 33(19), 8537–8559. <https://doi.org/10.1175/jcli-d-19-0696.1>
- Ban, N., Caillaud, C., Coppola, E., Pichelli, E., Sobolowski, S., Adinolfi, M., et al. (2021). The first multi-model ensemble of regional climate simulations at kilometer-scale resolution, part I: Evaluation of precipitation. *Climate Dynamics*, 57(1), 275–302. <https://doi.org/10.1007/s00382-021-05708-w>
- Bentsen, M., Bethke, I., Debernard, J. B., Iversen, T., Kirkevåg, A., Seland, Ø., et al. (2013). The Norwegian earth system model, NorESM1-M-Part 1: Description and basic evaluation of the physical climate. *Geoscientific Model Development*, 6(3), 687–720. <https://doi.org/10.5194/gmd-6-687-2013>
- Bettolli, M. L., Penalba, O. C., & Vargas, W. M. (2010). Synoptic weather types in the south of South America and their relationship to daily rainfall in the core crop-producing region in Argentina. *Australian Meteorological and Oceanographic Journal*, 60(1), 37–48. <https://doi.org/10.22499/2.6001.004>
- Boisier, J. P., Ciais, P., Ducharne, A., & Guimberteau, M. (2015). Projected strengthening of Amazonian dry season by constrained climate model simulations. *Nature Climate Change*, 5(7), 656–660. <https://doi.org/10.1038/nclimate2658>
- Boucher, O., Servonnat, J., Albright, A. L., Aumont, O., Balkanski, Y., Bastrikov, V., et al. (2020). Presentation and evaluation of the IPSL-CM6A-LR climate model. *Journal of Advances in Modeling Earth Systems*, 12(7), e2019MS002010. <https://doi.org/10.1029/2019ms002010>
- Butt, N., De Oliveira, P. A., & Costa, M. H. (2011). Evidence that deforestation affects the onset of the rainy season in Rondonia, Brazil. *Journal of Geophysical Research*, 116(D11), D11120. <https://doi.org/10.1029/2010JD015174>
- Caballero, C. B., Ruhoff, A., & Biggs, T. (2022). Land use and land cover changes and their impacts on surface-atmosphere interactions in Brazil: A systematic review. *The Science of the Total Environment*, 808, 152134. <https://doi.org/10.1016/j.scitotenv.2021.152134>
- Cai, W., McPhaden, M. J., Grimm, A. M., Rodrigues, R. R., Taschetto, A. S., Garreaud, R. D., et al. (2020). Climate impacts of the El Niño–southern oscillation on South America. *Nature Reviews Earth & Environment*, 1(4), 215–231. <https://doi.org/10.1038/s43017-020-0040-3>
- Chug, D., Dominguez, F., & Yang, Z. (2022). The amazon and La Plata river basins as moisture sources of South America: Climatology and intraseasonal variability. *Journal of Geophysical Research: Atmospheres*, 127(12), e2021JD035455. <https://doi.org/10.1029/2021jd035455>
- Cook, B. I., Mankin, J. S., Marvel, K., Williams, A. P., Smerdon, J. E., & Anchukaitis, K. J. (2020). Twenty-first century drought projections in the CMIP6 forcing scenarios. *Earth's Future*, 8(6), e2019EF001461. <https://doi.org/10.1029/2019ef001461>
- Correa, I. C., Arias, P. A., & Rojas, M. (2021). Evaluation of multiple indices of the South American monsoon. *International Journal of Climatology*, 41(S1), E2801–E2819. <https://doi.org/10.1002/joc.6880>
- Costa, M. H., & Pires, G. (2010). Effects of Amazon and Central Brazil deforestation scenarios on the duration of the dry season in the arc of deforestation. *International Journal of Climatology*, 30(13), 1970–1979. <https://doi.org/10.1002/joc.2048>
- Danabasoglu, G., Lawrence, D., Lindsay, K., Lipscomb, W., & Strand, G. (2019). *NCAR CESM2 model output prepared for CMIP6 CMIP historical*. Earth System Grid Federation. Version, 20190912.



- Debertoli, S., Dubreuil, N., Funatsu, V., Delahaye, F., de Oliveira, C. H., Rodrigues-Filho, S., et al. (2015). Rainfall patterns in the southern Amazon: A chronological perspective (1971–2010). *Climatic Change*, *132*(2), 251–264. <https://doi.org/10.1007/s10584-015-1415-1>
- de Souza Costa, C. E. A., Blanco, C. J. C., & de Oliveira-Júnior, J. F. (2020). IDF curves for future climate scenarios in a locality of the Tapajós Basin, Amazon, Brazil. *Journal of Water and Climate Change*, *11*(3), 760–770. <https://doi.org/10.2166/wcc.2019.202>
- Dias, C. G., & Reboita, M. S. (2021). Assessment of CMIP6 simulations over tropical South America. *Revista Brasileira de Geografia Física*, *14*(03), 1282–1295. <https://doi.org/10.26848/rbfg.v14.3.p1282-1295>
- Douville, H., Raghavan, K., Renwick, J., Allan, R. P., Arias, P. A., Barlow, M., et al. (2021). Water cycle changes. In V. Masson-Delmotte, P. Zhai, A. Pirani, S. L. Connors, C. Péan, S. Berger, et al. (Eds.), *Climate change 2021: The physical science basis. Contribution of working Group I to the sixth assessment report of the Intergovernmental Panel on climate change* (pp. 1055–1210). Cambridge University Press. <https://doi.org/10.1017/9781009157896.010>
- Eiras-Barca, J., Dominguez, F., Yang, Z., Chug, D., Nieto, R., Gimeno, L., & Miguez-Macho, G. (2020). Changes in South American hydroclimate under projected Amazonian deforestation. *Annals of the New York Academy of Sciences*, *1472*(1), 104–122. <https://doi.org/10.1111/nyas.14364>
- Espinoza, J. C., Arias, P., Moron, V., Junquas, C., Segura, H., Sierra-Pérez, J., et al. (2021). Recent changes in the atmospheric circulation patterns during the dry-to-wet transition season in south tropical South America (1979–2020): Impacts on precipitation and fire season. *Journal of Climate*, *34*, 9025–9042. <https://doi.org/10.1175/JCLI-D-21-0303.1>
- Espinoza, J. C., Garreaud, R., Poveda, G., Arias, P. A., Molina-Carpio, J., Masiokas, M., et al. (2020). Hydroclimate of the Andes part I: Main climatic features. *Frontiers of Earth Science*, *8*, 64. <https://doi.org/10.3389/feart.2020.00064>
- Espinoza, J. C., Ronchail, J., Guyot, J. L., Cochonneau, G., Naziano, F., Lavado, W., et al. (2009). Spatio-temporal rainfall variability in the Amazon basin countries (Brazil, Peru, Bolivia, Colombia, and Ecuador). *International Journal of Climatology: A Journal of the Royal Meteorological Society*, *29*(11), 1574–1594. <https://doi.org/10.1002/joc.1791>
- Espinoza, J. C., Ronchail, J., Marengo, J., & Segura, H. (2019). Contrasting north–south changes in Amazon wet-day and dry-day frequency and related atmospheric features (1981–2017). *Climate Dynamics*, *116*(9–10), 5413–5430. <https://doi.org/10.1007/s00382-018-4462-2>
- Eyring, V., Bony, S., Meehl, G. A., Senior, C. A., Stevens, B., Stouffer, R. J., & Taylor, K. E. (2016). Overview of the coupled model Intercomparison project phase 6 (CMIP6) experimental design and organization. *Geoscientific Model Development*, *9*(5), 1937–1958. <https://doi.org/10.5194/gmd-9-1937-2016>
- Fan, X., Miao, C., Duan, Q., Shen, C., & Wu, Y. (2020). The performance of CMIP6 versus CMIP5 in simulating temperature extremes over the global land surface. *Journal of Geophysical Research: Atmospheres*, *125*(18), e2020JD033031. <https://doi.org/10.1029/2020jd033031>
- Flato, G., Marotzke, J., Abiodun, B., Braconnot, P., Chou, S. C., Collins, W., et al. (2013). Evaluation of climate models. In *Climate change 2013: The physical science basis. Contribution of working Group I to the fifth assessment report of the Intergovernmental Panel on climate change* (pp. 741–866). Cambridge University Press.
- Fosser, G. S. K. P. B., Khodayar, S., & Berg, P. (2015). Benefit of convection permitting climate model simulations in the representation of convective precipitation. *Climate Dynamics*, *44*(1), 45–60. <https://doi.org/10.1007/s00382-014-2242-1>
- Fu, R., Yin, L., Li, W., Arias, P. A., Dickinson, R. E., Huang, L., et al. (2013). Increased dry season length over southern Amazonia in recent decades and its implication for future climate projection. *Proceedings of the National Academy of Sciences of the United States of America*, *110*(45), 18110–18115. <https://doi.org/10.1073/pnas.1302584110>
- Fujimori, S., Hasegawa, T., Masui, T., Takahashi, K., Herran, D. S., Dai, H., et al. (2017). SSP3: AIM implementation of shared socioeconomic pathways. *Global Environmental Change*, *42*, 268–283. <https://doi.org/10.1016/j.gloenvcha.2016.06.009>
- Funk, C., Peterson, P., Landsfeld, M., Pedreros, D., Verdin, J., Shukla, S., et al. (2014). The climate hazards infrared precipitation with stations—A new environmental record for monitoring extremes [Dataset]. *Scientific Data*, *2*(1), 150066. <https://doi.org/10.1038/sdata.2015.66>
- Garreaud, R. D. (2009). The Andes climate and weather. *Advances in Geosciences*, *22*, 3–11. <https://doi.org/10.5194/adgeo-22-3-2009>
- Giráldez, L., Silva, Y., Zubieta, R., & Sulca, J. (2020). Change of the rainfall seasonality over central Peruvian Andes: Onset, end, duration and its relationship with large-scale atmospheric circulation. *Climate*, *8*(2), 23. <https://doi.org/10.3390/cli8020023>
- Hersbach, H., Bell, B., Berrisford, P., Hirahara, S., Horányi, A., Muñoz-Sabater, J., et al. (2020). The ERA5 global reanalysis [Dataset]. *Quarterly Journal of the Royal Meteorological Society*, *146*(730), 1999–2049. <https://doi.org/10.1002/qj.3803>
- Hewitson, B., & Crane, R. (2002). Self-organizing maps: Applications to synoptic climatology. *Climate Research*, *22*, 13–26. <https://doi.org/10.3354/cr022013>
- Junquas, C., Vera, C., Li, L., & Le Treut, H. (2012). Summer precipitation variability over Southeastern South America in a global warming scenario. *Climate Dynamics*, *38*(9–10), 1867–1883. <https://doi.org/10.1007/s00382-011-1141-y>
- Kendon, E. J., Roberts, N. M., Senior, C. A., & Roberts, M. J. (2012). Realism of rainfall in a very high-resolution regional climate model. *Journal of Climate*, *25*(17), 5791–5806. <https://doi.org/10.1175/jcli-d-11-00562.1>
- Li, J., Huo, R., Chen, H., Zhao, Y., & Zhao, T. (2021). Comparative assessment and future prediction using CMIP6 and CMIP5 for annual precipitation and extreme precipitation simulation. *Frontiers in Earth Science*, *9*, 687976. <https://doi.org/10.3389/feart.2021.687976>
- Li, W., & Fu, R. (2004). Transition of the large-scale atmospheric and land surface conditions from the dry to the wet season over Amazonia as diagnosed by the ECMWF re-analysis. *Journal of Climate*, *17*(13), 2637–2651. [https://doi.org/10.1175/1520-0442\(2004\)017<2637:TOTLAA.2.0.CO;2](https://doi.org/10.1175/1520-0442(2004)017<2637:TOTLAA.2.0.CO;2)
- Marengo, J. A., Fisch, G. F., Alves, L. M., Sousa, N. V., Fu, R., & Zhuang, Y. (2017). Meteorological context of the onset and end of the rainy season in Central Amazonia during the GoAmazon2014/5. *Atmospheric Chemistry and Physics*, *17*(12), 7671–7681. <https://doi.org/10.5194/acp-17-7671-2017>
- Marengo, J. A., Jimenez, J. C., Espinoza, J. C., Cunha, A. P., & Aragão, L. E. O. (2022). Increased climate pressure on the agricultural Frontier in the Eastern Amazonia–Cerrado transition zone. *Scientific Reports*, *12*(1), 457. <https://doi.org/10.1038/s41598-021-04241-4>
- Marengo, J. A., Liebmann, B., Grimm, A. M., Misra, V., Silva Dias, P. D., Cavalcanti, I. F. A., et al. (2012). Recent developments on the South American monsoon system. *International Journal of Climatology*, *32*(1), 1–21. <https://doi.org/10.1002/joc.2254>
- Marengo, J. A., Souza, C. M., Jr., Thonicke, K., Burton, C., Halladay, K., Betts, R. A., et al. (2018). Changes in climate and land use over the Amazon region: Current and future variability and trends. *Frontiers in Earth Science*, *6*, 228. <https://doi.org/10.3389/feart.2018.00228>
- Monteverde, C., De Sales, F., & Jones, C. (2022). Evaluation of the CMIP6 performance in simulating precipitation in the Amazon river basin. *Climate*, *10*(8), 122. <https://doi.org/10.3390/cli10080122>
- Moon, S., & Ha, K. J. (2020). Future changes in monsoon duration and precipitation using CMIP6. *NPJ Climate and Atmospheric Science*, *3*(1), 45. <https://doi.org/10.1038/s41612-020-00151-w>
- Moron, V., Robertson, A. W., Qian, J. H., & Ghil, M. (2015). Weather types across the Maritime Continent: From the diurnal cycle to interannual variations. *Frontiers in Environmental Science*, *2*, 65. <https://doi.org/10.3389/fevns.2014.00065>
- Moron, V., Robertson, A. W., Ward, M. N., & Ndiaye, O. (2008). Weather types and rainfall over Senegal. Part II: Downscaling of GCM simulations. *Journal of Climate*, *21*(2), 288–307. <https://doi.org/10.1175/2007jcli1624.1>

- Müller, W. A., Jungclaus, J. H., Mauritsen, T., Baehr, J., Bittner, M., Budich, R., et al. (2018). A higher-resolution version of the Max Planck Institute Earth System Model (MPI-ESM1. 2-HR). *Journal of Advances in Modeling Earth Systems*, *10*(7), 1383–1413. <https://doi.org/10.1029/2017ms001217>
- Nobre, C. A., Obregón, G. O., Marengo, J. A., Fu, R., & Poveda, G. (2009). Characteristics of Amazonian climate: Main features. *Amazonia and global change*, *18*(6), 149–162. <https://doi.org/10.1029/2008gm000720>
- Olmo, M. E., & Bettolli, M. L. (2021). Extreme daily precipitation in southern South America: Statistical characterization and circulation types using observational datasets and regional climate models. *Climate Dynamics*, *57*(3–4), 895–916. <https://doi.org/10.1007/s00382-021-05748-2>
- Olmo, M. E., Espinoza, J. C., Bettolli, M. L., Sierra, J. P., Junquas, C., Arias, P. A., et al. (2022). Circulation patterns and associated rainfall over South Tropical South America: GCMs evaluation during the dry-to-wet transition season. *Journal of Geophysical Research: Atmospheres*, *127*(12), e2022JD036468. <https://doi.org/10.1029/2022jd036468>
- Orrison, R., Vuille, M., Smerdon, J. E., Apaéstegui, J., Campos, J. L. P., Cruz, F. W., & Della Libera, M. E. (2022). South American Monsoon variability over the last millennium in paleoclimate records and isotope-enabled climate models. *Climate of the Past Discussions*, *18*(9), 2045–2062.
- Ortega, G., Arias, P. A., Villegas, J. C., Marquet, P. A., & Nobre, P. (2021). Present-day and future climate over central and South America according to CMIP5/CMIP6 models. *International Journal of Climatology*, *41*(15), 6713–6735. <https://doi.org/10.1002/joc.7221>
- Paccini, L., Espinoza, J. C., Ronchail, J., & Segura, H. (2018). Intraseasonal rainfall variability in the Amazon basin related to large-scale circulation patterns: A focus on western Amazon–Andes transition region. *International Journal of Climatology*, *38*(5), 2386–2399. <https://doi.org/10.1002/joc.5341>
- Parsons, L. A. (2020). Implications of CMIP6 projected drying trends for 21st century Amazonian drought risk. *Earth's Future*, *8*(10), e2020EF001608. <https://doi.org/10.1029/2020ef001608>
- Pascale, S., Carvalho, L., Adams, D. K., Castro, C. L., & Cavalcanti, I. F. (2019). Current and future variations of the monsoons of the Americas in a warming climate. *Current Climate Change Reports*, *5*(3), 125–144. <https://doi.org/10.1007/s40641-019-00135-w>
- Pichelli, E., Coppola, E., Sobolowski, S., Ban, N., Giorgi, F., Stocchi, P., et al. (2021). The first multi-model ensemble of regional climate simulations at kilometer-scale resolution part 2: Historical and future simulations of precipitation. *Climate Dynamics*, *56*(11), 3581–3602. <https://doi.org/10.1007/s00382-021-05657-4>
- Rao, V. B., Franchito, S. H., Rosa, M. B., Govardhan, D., Figueroa, S. N., & Bhargavi, V. S. L. (2022). A changing climate Hadley cell induces a record flood in Amazon and another recorded drought across South Brazil in 2021. *Natural Hazards*, *114*(2), 1549–1561. <https://doi.org/10.1007/s11069-022-05437-1>
- Riahi, K., Van Vuuren, D. P., Kriegler, E., Edmonds, J., O'Neill, B. C., Fujimori, S., et al. (2017). The shared socioeconomic pathways and their energy, land use, and greenhouse gas emissions implications: An overview. *Global Environmental Change*, *42*, 153–168. <https://doi.org/10.1016/j.gloenvcha.2016.05.009>
- Rivera, J. A., & Arnould, G. (2020). Evaluation of the ability of CMIP6 models to simulate precipitation over Southwestern South America: Climatic features and long-term trends (1901–2014). *Atmospheric Research*, *241*, 104953. <https://doi.org/10.1016/j.atmosres.2020.104953>
- Ruiz-Vásquez, M., Arias, P. A., Martínez, J. A., & Espinoza, J. C. (2020). Effects of Amazon basin deforestation on regional atmospheric circulation and water vapor transport towards tropical South America. *Climate Dynamics*, *54*(9–10), 4169–4189. <https://doi.org/10.1007/s00382-020-05223-4>
- Segura, H., Junquas, C., Espinoza, J. C., Vuille, M., Jauregui, Y. R., Rabatel, A., et al. (2019). New insights into the rainfall variability in the tropical Andes on seasonal and interannual time scales. *Climate Dynamics*, *53*(1), 405–426. <https://doi.org/10.1007/s00382-018-4590-8>
- Sena, A. C. T., & Magnusdóttir, G. (2020). Projected end-of-century changes in the South American Monsoon in the CESM large ensemble. *Journal of Climate*, *33*(18), 7859–7874. <https://doi.org/10.1175/jcli-d-19-0645.1>
- Sierra, J. P., Espinoza, J. C., Junquas, C., Wongchuig, S., Polcher, J., Moron, V., et al. (2023). Impacts of land-surface heterogeneities and Amazonian deforestation on the wet season onset in southern Amazon. *Climate Dynamics*, *61*(9–10), 1–32. <https://doi.org/10.1007/s00382-023-06835-2>
- Sierra, J. P., Junquas, C., Espinoza, J. C., Segura, H., Condom, T., Andrade, M., et al. (2021). Deforestation impacts on Amazon–Andes hydroclimatic connectivity. *Climate Dynamics*, *58*(9), 2609–2636. <https://doi.org/10.1007/s00382-021-06025-y>
- Silva, C. H. L., Jr., Aragão, L. E. O. C., Anderson, L. O., Fonseca, M. G., Shimabukuro, Y. E., Vancutsem, C., et al. (2020). Persistent collapse of biomass in Amazonian forest edges following deforestation leads to unaccounted carbon losses. *Science Advances*, *6*(40), eaaz8360. <https://doi.org/10.1126/sciadv.aaz8360>
- Solman, S. A., & Menéndez, C. G. (2003). Weather regimes in the South American sector and neighbouring oceans during winter. *Climate Dynamics*, *21*(1), 91–104. <https://doi.org/10.1007/s00382-003-0320-x>
- Sousa, T. R., Schiatti, J., Ribeiro, I. O., Emílio, T., Fernández, R. H., ter Steege, H., et al. (2022). Water table depth modulates productivity and biomass across Amazonian forests. *Global Ecology and Biogeography*, *31*(8), 1571–1588. <https://doi.org/10.1111/geb.13531>
- Staal, A., Tuinenburg, O. A., Bosmans, J. H., Holmgren, M., van Nes, E. H., Scheffer, M., et al. (2018). Forest-rainfall cascades buffer against drought across the Amazon. *Nature Climate Change*, *8*(6), 539–543. <https://doi.org/10.1038/s41558-018-0177-y>
- Swart, N. C., Cole, J. N., Kharin, V. V., Lazare, M., Scinocca, J. F., Gillett, N. P., et al. (2019). The Canadian earth system model version 5 (CanESM5. 0.3). *Geoscientific Model Development*, *12*(11), 4823–4873. <https://doi.org/10.5194/gmd-12-4823-2019>
- Vera, C., Higgins, W., Amador, J., Ambrizzi, T., Garreaud, R., Gochis, D., et al. (2006). Toward a unified view of the American monsoon systems. *Journal of Climate*, *19*(20), 4977–5000. <https://doi.org/10.1175/jcli3896.1>
- Wainwright, C. M., Black, E., & Allan, R. P. (2021). Future changes in wet and dry season characteristics in CMIP5 and CMIP6 simulations. *Journal of Hydrometeorology*, *22*(9), 2339–2357. <https://doi.org/10.1175/jhm-d-21-0017.1>
- Wilks, D. S. (2019). *Statistical methods in the atmospheric sciences* (4th ed., p. 840). Elsevier.
- Wongchuig, S., Espinoza, J. C., Condom, T., Segura, H., Ronchail, J., Arias, P. A., et al. (2022). A regional view of the linkages between hydro-climatic changes and deforestation in the Southern Amazon. *International Journal of Climatology*, *42*(7), 3757–3775. <https://doi.org/10.1002/joc.7443>
- Ziehn, T., Chamberlain, M. A., Law, R. M., Lenton, A., Bodman, R. W., Dix, M., et al. (2020). The Australian earth system model: ACCESS-ESM1. 5. *Journal of Southern Hemisphere Earth Systems Science*, *70*(1), 193–214. <https://doi.org/10.1071/es19035>
- Zilli, M. T., & Carvalho, L. M. V. (2021). Detection and attribution of precipitation trends associated with the poleward shift of the South Atlantic Convergence Zone using CMIP5 simulations. *International Journal of Climatology*, *41*(5), 3085–3106. <https://doi.org/10.1002/joc.7007>